DOI: 10.13009/EUCASS2019-386

Experimental comparison of attitude controllers for nanosatellites

Bello, Álvaro[a]; Olfe, Karl[b]; Ezquerro, José Miguel[c]; Rodríguez, Jacobo[d] and Lapuerta, Victoria[e]

[a]Universidad Politécnica de Madrid, Edificio E-USOC, Campus de Montegancedo, M40 km 36-38, 28223, Pozuelo de Alarcón, Madrid, Spain, abello@eusoc.upm.es

[b]Universidad Politécnica de Madrid, Edificio E-USOC, Campus de Montegancedo, M40 km 36-38, 28223, Pozuelo de Alarcón, Madrid, Spain, kolfe@eusoc.upm.es

[c]Universidad Politécnica de Madrid, ETSIAE, Plaza Cardenal Cisneros, 3, 28040, Madrid, Spain, jm.ezquerro@upm.es

[d]Universidad Politécnica de Madrid, ETSIAE, Plaza Cardenal Cisneros, 3, 28040, Madrid, Spain, jacobo.rodriguez@upm.es

[e]Universidad Politécnica de Madrid, ETSIAE, Plaza Cardenal Cisneros, 3, 28040, Madrid, Spain, mariavictoria.lapuerta@upm.es

Nowadays, the attitude controllers based on artificial intelligence are being designed giving very good results compared with classical controllers. However, the performance comparisons made until now have been based on numerical simulations, being necessary experimental data and on-board tests.

In this work, a PID and a Fuzzy-logic based controllers have been developed for an educational nanosatellite (ESAT). Through the intensive use of the ESAT we have tested and compared the performance from an experimental point of view. Four performance indexes (accuracy, cost, stability and robustness) have been used to quantify the performance of each controller.

1. Introduction

The Attitude Determination and Control Subsystem (ADCS) design is a very important task in space missions [1]; accuracy, low power consumption, stability and robustness are the main requirements. Even though different control algorithms have been analysed in space industry, the most used controllers for small satellites are the classical Proportional Integral and Derivative (PID) controller [2] and the Linear Quadratic Regulator (LQR) controller [3]. The main reason for this tendency is that these controllers have been widely tested in space missions. Any change or improvement in the ADCS must be implemented very carefully to avoid any possible mission failure.

Previous works have analysed the use of intelligent controllers for applications in space missions based on Fuzzy logic [4-8] or learning algorithms like neural networks [9,10]. However, besides developing and implementing new controllers, it is necessary to compare them with the classical controllers by means of simulations and, of course, through experiments and on-board tests. In the work of Walker [7], the performances of a Fuzzy and a LQR controller were compared using simulations. In [11], a Fuzzy and a PID controllers were designed for a CubeSat specific mission, but its features (in terms of error and cost) were compared only through numerical simulations.

In this work the performance of a Fuzzy, a PID and a modified PID controller are compared experimentally by using the demonstrator and educational satellite called ESAT. The controllers have been designed for the ESAT specific test environment and their capabilities have been compared for the same attitude maneuvers.

This paper is organized as follows: In Section 2, the description of the experimental equipment is depicted. Section 3 describes the development of the 3 controllers for the ESAT. In Section 4, the main results of the maneuvers comparison are shown. Finally, in Section 5, the conclusions of this work are summarized.

DOI: 10.13009/EUCASS2019-386

2. System description

The ESAT has been developed as a flexible platform able to support training, development and testing activities on ground. One of the most powerful functionalities of the ESAT is the capability to design, implement and test different attitude control algorithms. This laboratory nanosatellite has many other functionalities that involve the rest of the typical subsystems of a satellite, but in this work only the characteristics that affect the ACS (Attitude Control System) are analysed.

2.1 Hardware Set-up

The key features of the ESAT ADCS are:

- Sensors: magnetometer, accelerometer and gyroscope.
- Actuators: two magnetorquers, momentum wheel.
- Turntable: which allows (quasi)free rotation in the *Z*-axis (Earth gravity axis).
- Microprocessor: execution loop at 4 [Hz].
- EPS (Electrical Power System): the 5.5 [V] line feeds the magnetorquers.

The following sections will highlight the most relevant characteristics influencing the study carried out in this work.

2.1.1 General System

As a laboratory satellite, ESAT incorporates the typical subsystems of a real satellite. The Electrical Power System (EPS) ensures the proper functioning of the ACS actuators by providing stable voltage in the feed lines. In case of low EPS batteries state of charge, the performance of the actuators may be reduced and affect the ACS consumption. Since power consumption is one of the parameters to evaluate the performance of the attitude control algorithm, tests have always been carried out with similar EPS batteries states of charge so that the possible influence is minimized.

Another item affecting the system is the Turntable, which allows ESAT to rotate on the *Z*-axis. It introduces an external disturbance torque in the system that substantially differentiates the rotation of the ESAT and the real free rotation of a satellite in orbit. The main sources of this friction torque are:

- The union between the Turntable and the Vertical Support (see Figure 1).
- The aerodynamic drag between the structure of the whole set and the air of the atmosphere.

To overcome this friction torque, it is necessary to strengthen the actions of the magnetorquers. This is achieved by aligning two neodymium magnets on both sides of the Turntable (see Figure 1). This generates a (quasi)uniform magnetic field of a higher order of magnitude than the Earth magnetic field in the vicinity of the ESAT. It should be kept in mind that the field generated by two dipoles is not completely uniform so the forces of the magnetorquers depend slightly on the attitude of the ESAT during the rotation around the *Z*-axis. The points of minimum available torque are in the following Euler angles:

$$\phi = 0\ ;\ \theta = 0\ ;\ \varphi = \frac{\pi}{4} + \frac{k \cdot \pi}{2} \text{ with } k = -2, -1, 0, 1$$

Being:

$$\phi \equiv roll\ angle\ [rad];\ \theta \equiv pitch\ angle\ [rad];\ \varphi \equiv yaw\ angle\ [rad]$$

In the ADCS processor software, the magnetic field is assumed uniform. This means that the attitude determination algorithm will make small mistakes when calculating the actual attitude of the satellite. This phenomenon is common in real satellites due to the fact that the real terrestrial magnetic field differs slightly from the most used theoretical models [12] and differs markedly in certain singular points.

The microprocessor that executes the ADCS code is an STM32. This family of microprocessors is powerful enough to run a control loop every 250 [ms]. However, the telemetry packets that arrive at the communication server are formed and sent every 1 [s]. It is important to keep this in mind because oscillations may be lost because of sampling frequency.

DOI: 10.13009/EUCASS2019-386

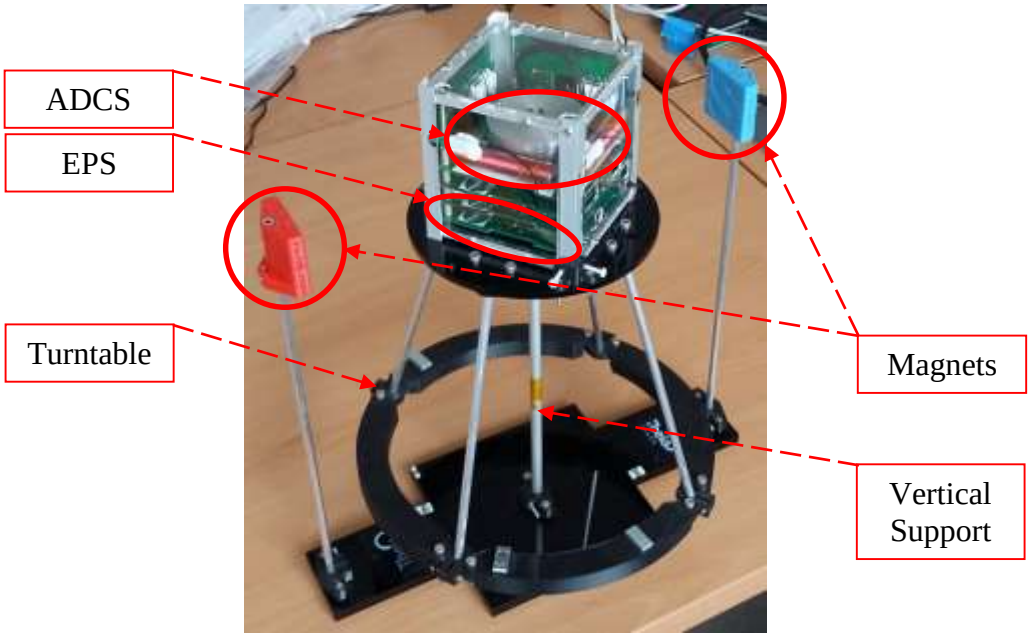

Figure 1: Experimental set-up: nanosatellite, turntable, magnets and support (picture courtesy of Theia Space).

2.1.2 Reference frames and Sensors

The first reference system is bound to the satellite, rotates in solidarity with the ESAT-Turntable set and is referred as "body reference frame" (BRF). This system is centered in the mass center of the assembly and its axes are aligned with the principal axes of inertia in such a way that the magnetorquers are parallel to the *X* and *Y* axes. The positive direction of the *Z*-axis is ascending in nominal attitude; that is, making it a right-handed reference system (see Figure 2). The second reference system is similar to the BRF but the *X*-axis is aligned with the magnetic field and the *Z*-axis is aligned with the minus acceleration of gravity; that is, aligned with the normal force (see Figure 2). Due to the characteristics of this reference frame it will be referred as the "inertial reference frame" (IRF).

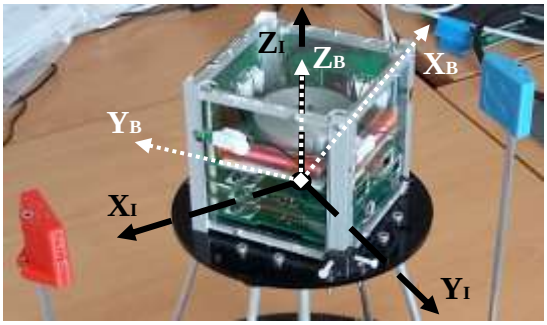

Figure 2: Reference frames: inertial (IRF) in black dashed and body (BRF) in white dotted.

Quaternions have been used for the attitude parameterization of the ESAT (see [13] for more detail about quaternion definition). It is important to know that the attitude of the satellite has been represented by quaternions because the error signal (which is one of the inputs of the controllers) depends on this parameterization. The quaternion error is defined as the product of quaternions between the reciprocal of the current quaternion and the desired quaternion. The error signal is defined as the vector part of the error quaternion as in the following equations:

$$q_{ERROR} = (q_{SAT})^{-1} * q_{TARGET}\,;\ \vec{e} = \mathrm{Im}(q_{ERROR}) \qquad \textbf{(1)}$$

Being:

$q_{ERROR} \equiv$ Error quaternion; $q_{SAT} \equiv$ Current quaternion;

$q_{TARGET} \equiv$ Target quaternion, $\vec{e} \equiv$ Error vector.

DOI: 10.13009/EUCASS2019-386

The ESAT could use various sensors for attitude determination, some of which are redundant. For the tests analysed in this work, the measurements collected by the following sensors were used:

- Magnetometers: to measure the direction of the magnetic field generated by the magnets.
- Gyroscopes: to measure the angular speed of rotation in all the axes.
- Accelerometers: to measure the direction of the gravitational vector.

To determine the attitude of the ESAT, the Q-method has been implemented using magnetometers and accelerometers [14]. In this work, the algorithms used for attitude determination will not be described in depth. However, it is important to point out that gyro measurements have been used as a substitute for the attitude derivative. By doing this, it is possible not to overload the processor with expensive numerical approximations and to have better approximations of the derived function. It is also important to keep in mind that the gyro signal is expressed in degrees per second [deg/s].

2.1.3 Actuators

ESAT has two types of actuators: two magnetorquers and one momentum wheel. In this paper we will focus on the usage of magnetorquers because they are capable of introducing external torque into the system. The reaction wheel only exchange torque within the system, and due to the existence of a friction torque, the use of the wheel inevitably leads to saturation. This generates a series of drawbacks that hinder the systematic analysis of the results pursued in this work. The equation of the performance of the magnetorquer is well known:

$$\vec{T}_{MAG} = \vec{m} \times \vec{B} \tag{2}$$

Being:

$\vec{T}_{MAG} \equiv$ Magnetic torque; $\vec{m} \equiv$ Dipole moment; $\vec{B} \equiv$ Magnetic field.

However, the control variable of the magnetorquer from the ADCS point of view is the percentage of operation between the values -100 and 100 [%]. The control drivers of the magnetorquers receive the command from the attitude control system and transform that percentage of operation into a polarity (positive or negative) and a current through the magnetorquer. This current modulates the maximum dipole moment that can be generated using: Pulse Width Modulation (PWM), so the real control variable is the dipole moment. For the reasons explained earlier, the external magnetic field is not completely uniform in all positions, meaning that the torque generated is not as well.

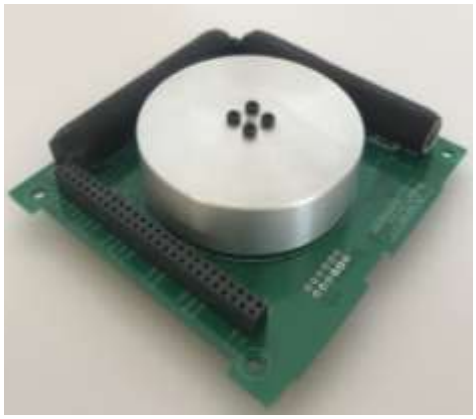

Figure 3: Image of the ADCS board with the actuators: wheel and magnetorquers (courtesy of Theia Space).

2.2 System equations analysis

Once the most important elements are known, the dynamics of the system can be modelled in a simple way. Considering the whole set as a rigid solid with axial symmetry around *Z*-axis, it is possible to particularize Newton second law in the body reference frame obtaining:

$$\text{Rigid Body:} \quad \sum \vec{T}_{EXT}^{BRF} = \frac{d\vec{L}_{INT}}{dt} = \bar{I}_{SAT}^{BRF} \frac{d\vec{\omega}_{SAT}^{BRF}}{dt}$$

$$\text{Axial Symmetry:} \quad T_{MAG}^{Z} + T_{FRIC}^{Z} = I_{SAT}^{Z} \frac{d\omega_{SAT}^{Z}}{dt} \tag{3}$$

DOI: 10.13009/EUCASS2019-386

Being:

$\vec{T}_{EXT}^{BRF}$ ≡ External torque in BRF; $\vec{L}_{INT}$ ≡ Internal angular momentum;

$\bar{I}_{SAT}^{BRF}$ ≡ Inertia tensor in BRF; $\vec{\omega}_{SAT}^{BRF}$ ≡ Angular speed in BRF.

T_{MAG}^{Z} ≡ Magnetic torque in Z-Axis; T_{FRIC}^{Z} ≡ Frictional torque in Z-Axis;

I_{SAT}^{Z} ≡ Z-Axis moment of inertia; ω_{SAT}^{Z} ≡ Angular speed in Z-Axis.

Observing the Eq. 3 it is confirmed that the dynamics of the system are closely linked to the friction torque. This torque is hard to model because it is composed of two contributions: the Turntable-Vertical Support junction friction and the aerodynamic drag. The aerodynamic drag has little relevance and only acts when the assembly is in motion. In general, the friction torque can be modelled as a time-independent constant [15]. However, it should be noted that these constants vary considerably depending on whether the assembly is moving or not. This is due to the differences of the static and dynamic friction coefficients. The friction between moving surfaces is generally lower, but the additional contribution of the aerodynamic drag should not be forgotten. The static friction torque generates an interesting problem for the control: the controllers may be commanding a non-zero action to the magnetorquers and yet receive no movement response from the system. In addition to this problem, there is the phenomenon of the joint wear, causing slight differences in those coefficients depending on the rotation direction and small changes over time because of repeated use.

Knowing this, the magnetic torque remains as the control torque. This is the key variable to be controlled using different strategies: one focused on classical control theory (PID) and another one using modern concepts (Fuzzy).

3. Controllers development

The ADCS execution loop can be summarized using the block diagram shown in Figure 4. It is important to note again that this loop is evaluated at 4 [Hz]. The following sections show the differences in the control block design.

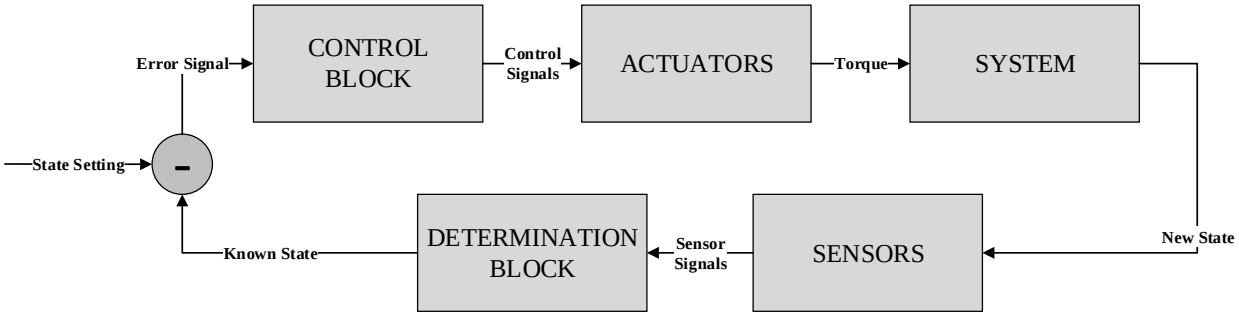

Figure 4: General overview of the ADCS loop.

3.1 Sugeno Fuzzy Controller

All the controllers shown in the next sections share a similar structure in terms of the control process (see Figure 5):

- Usage of three inputs for the whole controller: the Z component of the error vector (see Eqs. 1) called "Z error signal", the Z component of the gyro measurement vector called "Z gyro signal" and the magnetometer measurement vector called "Magnetic field 3D".
- Usage of two inputs for the control system: "Z error signal" and "Z gyro signal".
- Generation of the control torque needed: they combine the output of the control system, called "Z torque needed", with null variables.
- Calculation of the actuation required in both magnetorquers: they perform the cross product of the "Torque needed 3D" with the magnetic field to get the required X and Y magnetorquers commands.

For the fuzzy controller design it has been decided to use a Sugeno type inference structure [16] which is more intuitive, easier to calibrate and requires less computational effort when compared to e.g. a Mamdani inference. This choice influences, above all, the implication block and the aggregation of the rule outputs before the defuzzification phase

DOI: 10.13009/EUCASS2019-386

(see Figure 5). In order to understand the calibration parameters chosen for the controller, the operating loop of the fuzzy controller will be briefly explained.

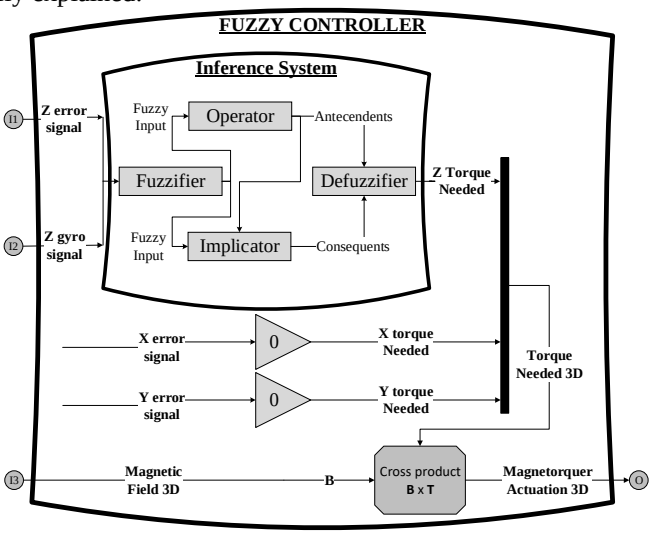

Figure 5: Block diagram of the Fuzzy Controller.

For both inputs five trapezoidal membership functions have been used to not saturate the capabilities of the microprocessor and, at the same time, to achieve enough distinction between the linguistic criteria. The values assigned to each of the fuzzy criteria are the result of a semi-automatic calibration process. By repeating and analysing the controller response the final value of the membership functions parameters have been adjusted.

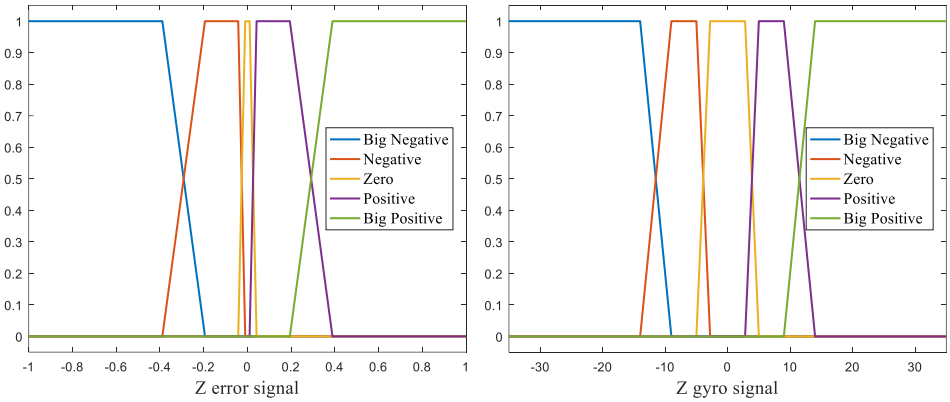

Figure 6: Input membership functions of the Fuzzy controller.

When the inputs are evaluated in the Fuzzifier, it is assigned a degree to each of the membership functions representing each percentage of fuzzy criteria veracity (see Figure 6). The outputs of the fuzzification are vectors of five members. These outputs are used by the rule block to evaluate each rule. This process is the most computationally expensive since the number of rules and operations is usually high. The rules have the following structure:

$$\textit{if}\ \ (\text{Input\_1=Big negative})\ \ \&\ \ (\text{Input\_2 = Big negative})\ \ \textit{then}\ \ (\text{Output\_1 = Big Positive})$$

For each rule defined in the controller database, the following steps are executed (see Figure 7):

- Calculate and regulate the antecedent:

The numerical values of the inputs are combined using the fuzzy logic operators. All database rules include an **AND** operator between the two inputs. The fuzzy operation chosen for AND type combinations is the product. Depending on the relative importance of the rules it is possible to assign them a weight between 0 and 1. In this case the relative weight of all the rules is the same and equal to 1.

- Calculate the consequent: it is executed in two steps.
  - 1st Step - Calculate the degree of membership of the rule output:

The membership functions of the output variables in a Sugeno type system are slightly different. They are expressed according to the degrees of membership of the input variables and have the form of polynomials:

DOI: 10.13009/EUCASS2019-386

$$y_k = K_0 + K_{11}\cdot x_1 + K_{12}\cdot x_1^2 + ... + K_{21}\cdot x_2 + K_{22}\cdot x_2^2 + ... + K_{nm}\cdot x_n^m$$

Being:

$y_k \equiv$ Membership degree of the rule k output; $x_i \equiv$ Membership degree of the input i;

$K_{ij} \equiv$ Multiplier of the input i with exponent j.

If the input multipliers are null, these output membership functions are known as singletons which is what it has been used in this work. Therefore, each rule output degree of membership is one of the numerical values specified in Table 1.

Table 1: Fuzzy singletons used for the output.

Fuzzy criteria	Big Negative	Negative	Zero	Positive	Big Positive
Z torque needed (K_0)	-1	-0.8	0	0.8	1

- 2nd Step - Implicate the rule output:

Once the antecedent and the output degree of membership have been calculated, the consequent of the rule is calculated using the implication method. Again, the function chosen for the implication is the product.

- Aggregate the result:

The antecedent and consequent are known as the output of each of the rules. In Sugeno type systems, these two variables are numerical values. Aggregation in a Sugeno type systems simply consists of saving these variables for later use in the defuzzification block (see Figure 7).

Therefore, we have just seen that the entries of the rule block are two diffuse variables (in this case 5 numeric values for each entry) and the outputs are two aggregated variables which contain all the antecedents and consequents of each rule. These variables are the inputs of the defuzzification block which, using the appropriate method, calculates the output of the inference system. The function chosen for defuzzification is the weighted average of all the rule outputs which is commonly used in Sugeno systems. Therefore the output is calculated with the expression:

$$Output = \frac{\sum_{i=1}^{N} Consequent_i}{\sum_{i=1}^{N} Antecedent_i} = \frac{\sum_{i=1}^{N} Antecedent_i \cdot y_i}{\sum_{i=1}^{N} Antecedent_i}$$

Being:

$N \equiv$ Total number of rules; $y_i \equiv$ Output membership degree of the rule i.

Now that the inference process is stated, the calibration parameters of the fuzzy controller are:

- Form and parameters of the input membership functions (see Figure 6).
- Number and content of the rules (see Table 2).
- Parameters of the output membership functions, in this case the singleton values (see Table 1).

Table 2: Summary of the rules included in the controller database. The contents of the table represents all combinations of AND operations between both fuzzy inputs and the output singleton assign to that rule.

		Z gyro signal				
		Big Negative	Negative	Zero	Positive	Big Positive
Z error signal	Big Negative	1	1	1	0.5	0
	Negative	1	1	0.5	0	0.5
	Zero	0.5	0.5	0	-0.5	-0.5
	Positive	-0.5	0	-0.5	-1	-1
	Big Positive	0	-0.5	-1	-1	-1

As can be deduced from the high number of degrees of freedom, a fuzzy controller is highly adaptable to the system. It seems that having a high number of parameters makes the calibration process harder; however, due to the ease of associating linguistic terms with specific aspects of the system, calibration is greatly facilitated. All these parameters must be specified before the controller is put into operation. For this reason, the controller strongly benefits from the expert knowledge of the designer.

DOI: 10.13009/EUCASS2019-386

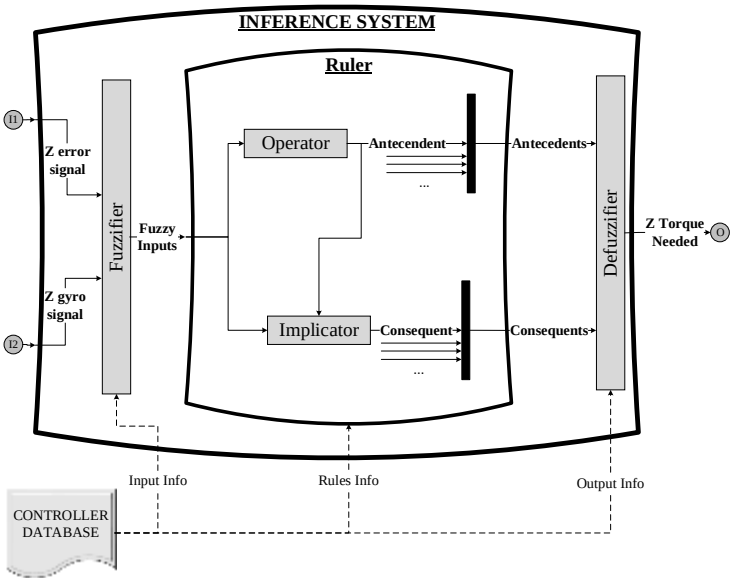

Figure 7: Block diagram of the Sugeno Inference System.

3.2 PID & PID modified controllers

The general structure of the PID controller is the same as explained in the first paragraph of section 3.1 Sugeno Fuzzy Controller. The significant changes are within the block called "PID System" (see Figure 8). In this case the structure of that block is much simpler and can be explained briefly with the diagram below.

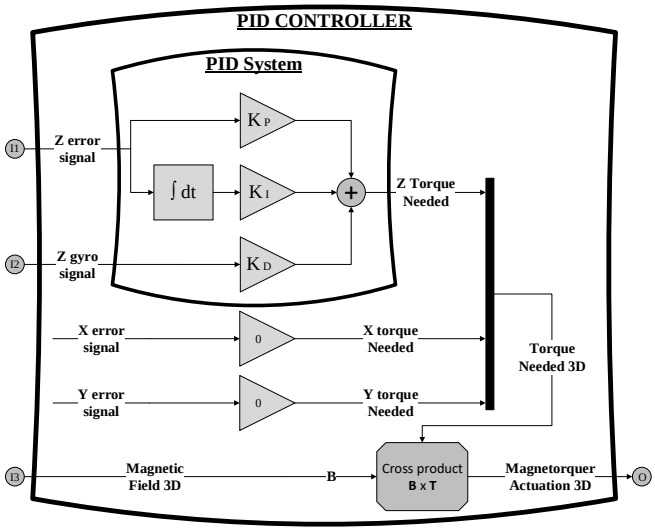

Figure 8: Diagram of the classic PID controller.

The operation of a PID controller is well known and a detailed analysis of its operation is not within the scope of this work. It is worth mentioning that the error derivative signal has been replaced by the gyro readings. This decision, which has also been applied in the Fuzzy system, has been taken for two main reasons:

- Availability: ESAT includes among its features a good angular velocity sensor.
- Computational savings: approximating the error derivative requires storing several values from the past iterations as well as performing additional operations that impair the computational efficiency of the control loop.

The general PID control equation applied to this system takes the following form:

$$Output(t) = K_P \cdot e_Z(t) + K_I \cdot \int e_Z(t)dt + K_D \cdot \omega_Z(t) \quad \textbf{(4)}$$

DOI: 10.13009/EUCASS2019-386

Being:

Output ≡ Z-Torque needed; K_P, K_I, K_D ≡ Proportional, integral and derivative gains

$e_Z = \vec{e}(3)$ ≡ Z-Component of the error; $\omega_Z = \vec{\omega}_{SAT}^{BRF}(3)$ ≡ Z-Component of the angular speed;

As can be deduced from Eq. 4, the calibration parameters that control PID performance are the gains: $\mathbf{K_P}$, $\mathbf{K_I}$ and $\mathbf{K_D}$. The calibration process in a PID may seem simple, but the system response when several gains are modified simultaneously is not intuitive. There are methodologies for calibrating PID controllers but many of them are manual, tedious and do not usually apply to all systems. The values associated with the controller gains used in this article are the result of a semi-automatic calibration process consisting of a repeated analysis to the response to 180 [deg] steps in the error signal. A problem typically manifested by PID controllers is that they execute correctly the calibration maneuver but do not perform well when disturbances change the nominal situation.

Some of the most recurring problems in this type of controllers are related to the integral signal. Commanding a step generates an undesired initial increase in the integral function. This accumulation can be mitigated in several ways:

- Drastically reducing integral gain, $\mathbf{K_I}$:

This causes the controller being slow (taking a long time to converge) and not accurate during a large part of the maneuver (except for the maneuver for which they have been calibrated). However, they ensure convergence to the commanded state. Another problem is that longer times penalize the energy consumed making them uncompetitive.

- Adjusting the overshoot:

The only way to counteract the initial increase in the values of the integral function is to make use of an overshoot. This generates faster controllers which arrive earlier close to the commanded state. However, they waste a lot of effort nullifying the initial step so they are comparatively inefficient.

- Overriding the integral function:

Another way to deal with this problem is to override the integral function each time the error function changes its sign. This allows to drastically increase the relative value of the integral gain making a more agile controller which responds earlier to situations of unbalance. It is a good method to deal with calibration problems posed by a PID when commanding different maneuvers. However, this approach introduces concepts which are not related to the PID theory.

While introducing some drawbacks, the integral signal also provides one of the most characteristic advantages of PID controllers. Although the gain values are not optimal for a specific command, the integral signal allows converging to the commanded state if the time is long enough. For this reason, the residual error is usually small. Because a classical PID controller should not override the integral function, two situations have been studied separately:

- Classic PID calibrated for 180 [deg] maneuvers with overshoot.
- Modified PID calibrated for 180 [deg] maneuvers that resets the integral function.

The Figure 9 highlights the differences between the classic PID and the modified one implemented in this article.

4. Experimental results

The calibration process for all controllers (Fuzzy, classic and modified PID) has been the same: execute a 180 [deg] maneuver, analyse the system response, change the necessary parameters and repeat the procedure until converging towards a satisfactory result. Once the controllers have been calibrated, a series of different maneuvers have been performed to compare the controllers in terms of: fastness (time needed to converge), accuracy (residual error after the stabilization phase), consumption (electrical energy consumed during the maneuver), and robustness (variation of the response to disturbances in the system).

The maneuvers chosen can be grouped into two main groups: turns of 179 [deg] and 90 [deg]. An amplitude of 179 [deg] has been chosen in order to avoid ambiguity in rotation directions. Although they are grouped in terms of their amplitude, it must be kept in mind that not all the maneuvers are exactly the same. Some of the sources of these differences lie in the following aspects:

- Uneven wear of the Turntable-Vertical Support joint (see section 2.2 System equations analysis): the friction coefficients have different values in one rotation direction or the other.
- Non-uniform magnetic field (see section 2.1.1 General System): the magnetic field is not uniform in all ESAT positions, so the initial and final state are also relevant when executing a maneuver.

The experimental data generation procedure is summarized in Table 3.

DOI: 10.13009/EUCASS2019-386

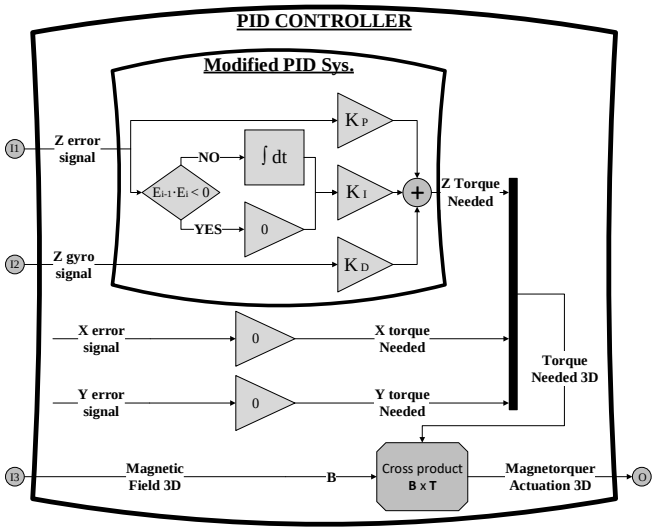

Figure 9: Diagram of the modified PID controller.

Table 3: Experimental procedure executed.

Turn amplitude [deg]	Turn direction [+/-]	Initial yaw [deg]	Final yaw [deg]	Maneuver [#]
90	+	0	90	1
		90	+/-180	2
		+/-180	-90	3
		-90	0	4
	-	0	-90	5
		-90	+/-180	6
		+/-180	+90	7
		+90	0	8
179	+	0	+179	9
	-	+179	0	10
		0	-179	11
	+	-179	0	12
	-	+/-180	+1	13
	+	+1	+/-180	14
		+/-180	-1	15
	-	-1	+/-180	16

4.1 Short maneuvers (90 degrees)

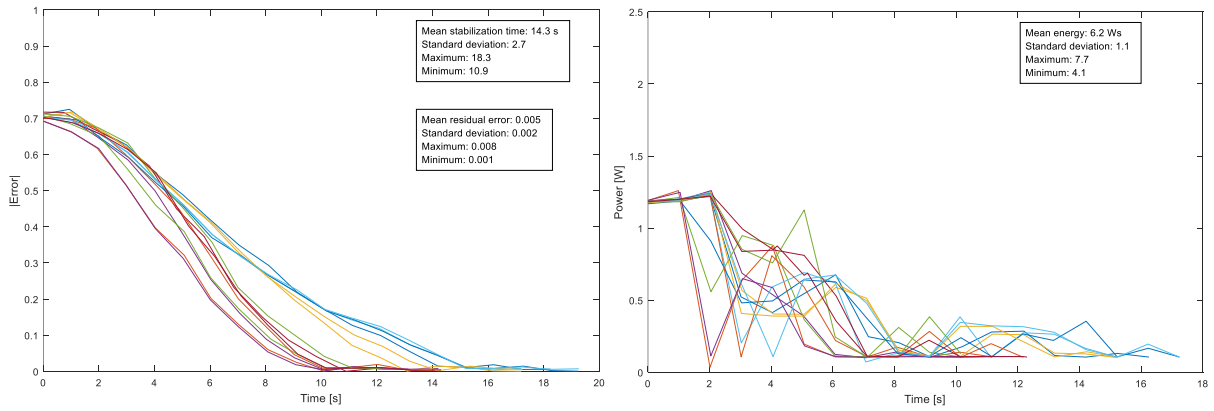

Figure 10: Absolute value of the Fuzzy error (left) and power consumed by the EPS (right) versus time. Maneuver amplitude of 90 [deg]. Each line plot corresponds to one of the maneuvers defined in Table 3.

DOI: 10.13009/EUCASS2019-386

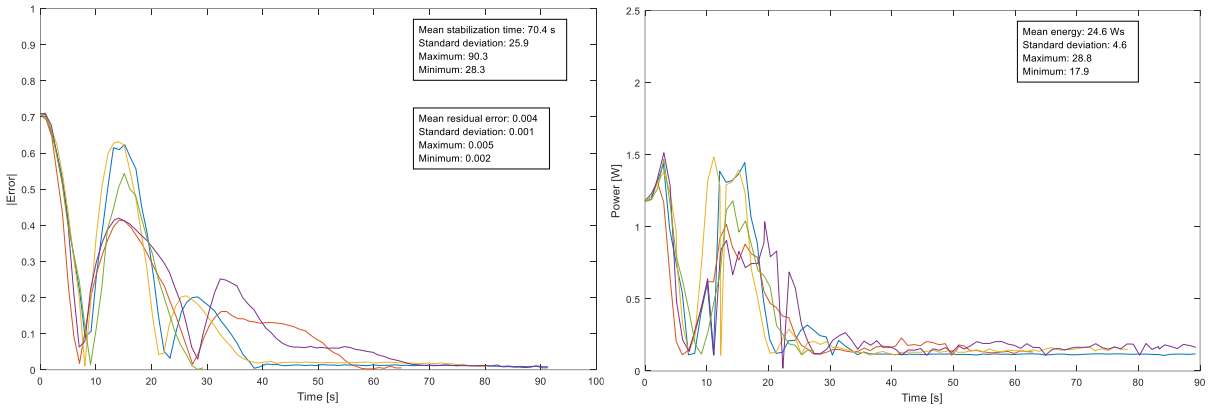

Figure 11: Absolute value of the classic PID error (left) and power consumed by the EPS (right) versus time. Maneuver amplitude of 90 [deg]. Each line plot corresponds to one of the maneuvers defined in Table 3.

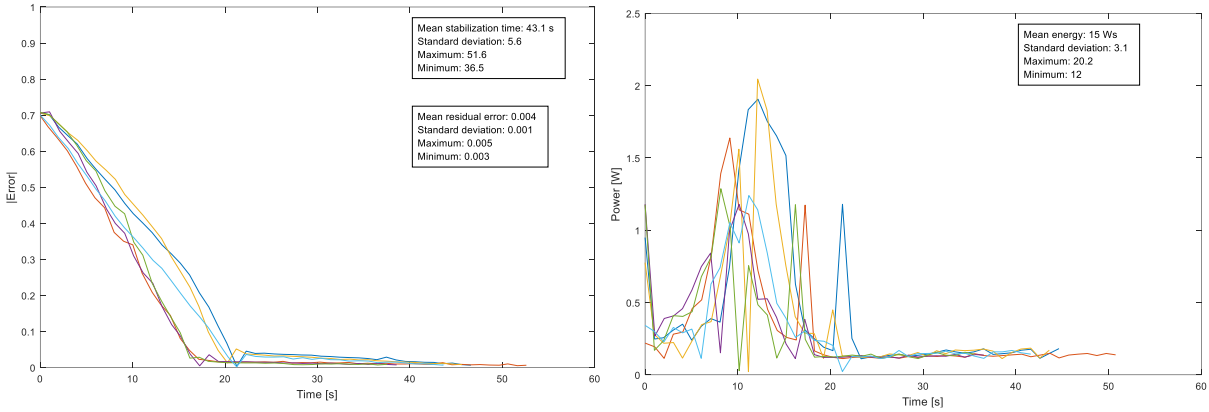

Figure 12: Absolute value of the modified PID error (left) and power consumed by the EPS (right) versus time. Maneuver amplitude of 90 [deg]. Each line plot corresponds to one of the maneuvers defined in Table 3.

As can be seen, two groups of maneuvers can be differentiated according to the slopes observed in the error plot (see Figure 10 left): the positive and negative turn direction maneuvers. In all of them a slight change of slope can be observed when the error ≈ 0.2. This change corresponds to the change of fuzzy criteria between the "Big Negative/Positive" and "Negative/Positive" functions (see Figure 6). The next sudden change of slope is in the immediate vicinity of the commanded state when the error ≈ 0.01. This change in controller behaviour is due to the transition between the "Negative/Positive" and "Zero" error membership functions.

In the case of the classic PID controller (Figure 11), it can be observed that the fact of using an overshoot to achieve a quick response penalizes the maneuver in all senses. In addition to this aspect it must be taken into account that all controllers were calibrated for 180 [deg] maneuvers; therefore, when trying to execute a 90 [deg] maneuver this controller is not able to efficiently manage it. Another noteworthy aspect is the great variability between the different maneuvers. In general, all of them cross the commanded state twice before stabilizing; however, while in one direction of rotation they manage to correctly override the integral function, in the other direction, they need a remarkably long error constant phase to start correcting the final state. This is because they have not been able to stabilize with a reasonably small integral function value. Finally, it should be noted that the fastest maneuver took less than one third of the slowest and less than half of the average. This means that the behaviour of the PID controller is severely affected by changing external circumstances (magnetic field and friction coefficients).

In the modified PID controller (Figure 12), a radically different behaviour is observed. The most abrupt change of slope is observed in the immediate vicinity of the commanded state when the error ≈ 0.03. This is due to the fact that when the error function changes its sign, the controller cancels the integral function deleting the information of the first seconds. This greatly improves the behaviour of the PID controller making it more efficient in terms of time and consumption. Interestingly, in this case, the graphs are also grouped into two groups with slightly different slopes. As with the fuzzy controller, differences in the friction coefficient according to the direction of rotation generate differences in the slopes of the error plots. Due to the frictional torque, it is necessary to generate a relatively high torque (between 50 and 70% depending on the exact position of the ESAT). This means that the integral function must be able to change its value with sufficient agility to respond to those situations. If the value of the integral gain, $\mathbf{K_I}$, is

DOI: 10.13009/EUCASS2019-386

increased, the controller responds with greater actuation to these differences; however, it will need more time to stabilize due to oscillations around the commanded state. This problem arises, above all, when executing maneuvers for which the controller has not been calibrated and it has not an easy solution. It is possible to introduce a second intelligent criterion that overrides all actuation when the system is close to the commanded state. However, this nullifies the main advantage of using a PID: it always converges to the commanded state with almost zero error.

4.2 Long maneuvers (180 degrees)

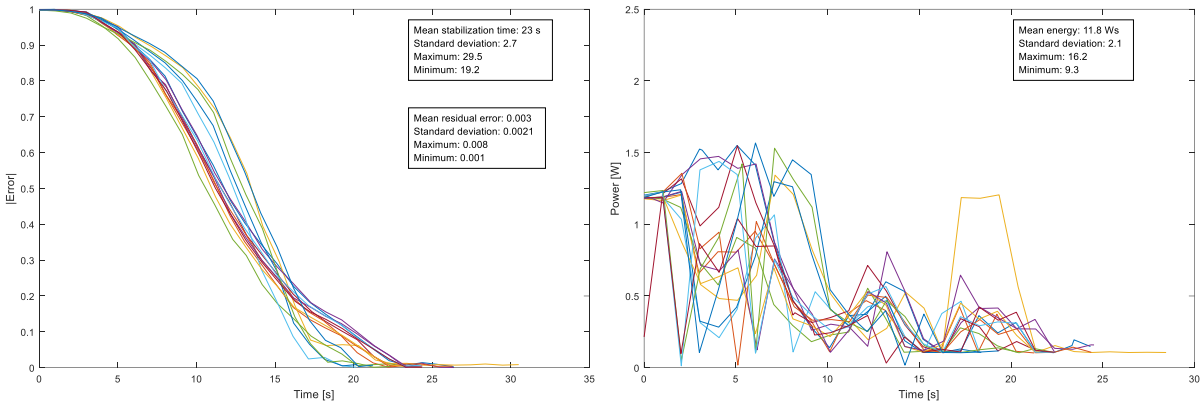

Figure 13: Absolute value of the Fuzzy error (left) and power consumed (right) versus time. Maneuver amplitude of 180 [deg]. Each line plot corresponds to one of the maneuvers defined in Table 3.

In the 180 [deg] maneuvers for the fuzzy controller (Figure 13), the same phenomenon is observed as in the short maneuvers: depending on the rotation direction, the error profile varies slightly. It can also be observed that in one direction the initial acceleration is lower. In these maneuvers the first change of slope is governed by the transition in the gyro signal between the "Negative/Positive" and "Big Negative/Positive" membership functions. When the controller detects that the speed is not big enough it suddenly forces an acceleration of the system (at around 12 [s] of maneuver). The next big slope change observed in these maneuvers is around $|error| \approx 0.1$ which is when the error belongs only to the domain of the “Negative/Positive” membership function (around the 17 [s] of maneuver). This is because one of the rules states the need to counteract the error signal when the derivative is too high in spite of being against the nominal performance of the controller.

However, in the other direction of rotation, since the initial acceleration is good, the initial abrupt change of slope is not appreciated. In these maneuvers the main change of slope is observed when the error signal ≈ 0.2. As mentioned before, this change is due to a transition of the error value between "Negative/Positive" and "Zero" domains.

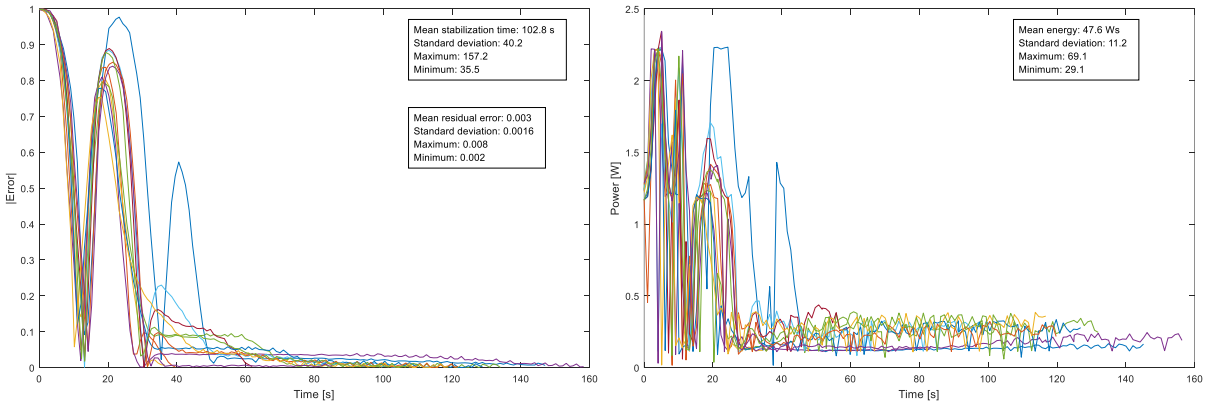

Figure 14: Absolute value of the classical PID error (left) and power consumed by the EPS (right) versus time. Maneuver amplitude of 180 [deg]. Each line plot corresponds to one of the maneuvers defined in Table 3.

All the aspects that were highlighted in the previous section on the problems of the classic PID controller are also present in Figure 14. It is worth noting the increased variability between the different maneuvers. While the calibration maneuver (maneuver #9 in Table 3) is executed in about 35.5 [s] consuming 29.1 [Ws], the average of the rest of maneuvers multiplies by two or three these values. In fact, the 180 [deg] calibration maneuver executes it more

DOI: 10.13009/EUCASS2019-386

efficiently than some of the maneuvers shown in the previous section despite being less demanding maneuvers (see Figure 11). All these aspects confirm one of the main problems of the PID: it is very sensitive to variations in operating conditions.

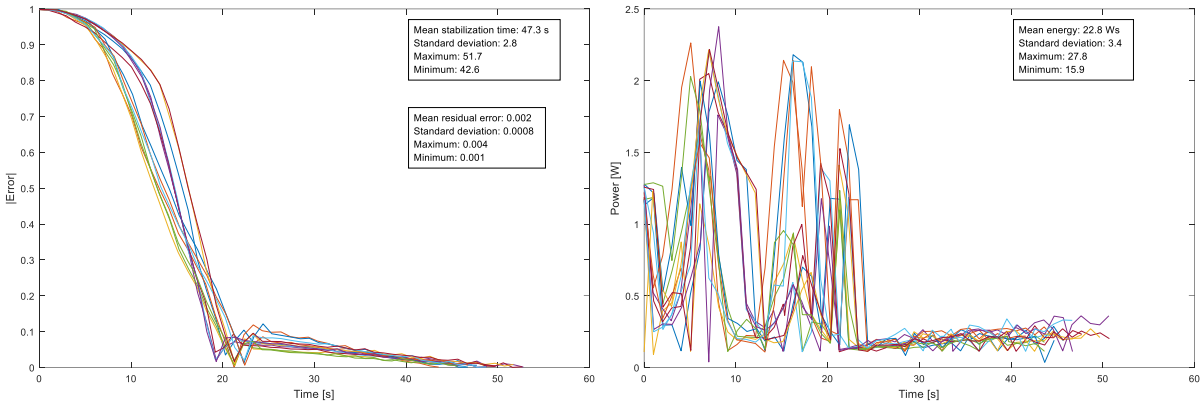

Figure 15: Absolute value of the modified PID error (left) and power consumed by the EPS (right) versus time. Maneuver amplitude of 180 [deg]. Each line plot corresponds to one of the maneuvers defined in Table 3.

As for the behaviour of the modified PID in the 180 [deg] maneuvers, nothing new can be highlighted. Everything mentioned in the previous section applies to these plots. It should be noted that the increase in convergence time is reasonably small which indicates that most of the maneuvering time is used to converge when the error is small. In the case of Figure 15 the characteristic times are equally distributed. However, in the short maneuvers (see Figure 12) it could be appreciated that the convergence time when the error is small is comparatively longer.

4.3 Performance comparison

The most relevant results obtained are grouped in Table 4 to facilitate its comparison:

Table 4: Experimental results summary.

Maneuvers [deg]	Evaluation variable	Fuzzy	PID classic	PID modified	Best
90	Mean convergence time [s]	14.3	70.4	43.1	Fuzzy
	Min. convergence time [s]	10.9	28.3	36.5	Fuzzy
	Max. convergence time [s]	18.3	90.3	51.6	Fuzzy
	Mean residual error	5e-3	4e-3	4e-3	PIDm
	Mean power consumed [W·s]	6.2	24.6	15.0	Fuzzy
	Min. power consumed [W·s]	4.1	17.9	12.0	Fuzzy
	Max. power consumed [W·s]	7.7	28.8	20.2	Fuzzy
180	Mean convergence time [s]	23.0	102.8	47.3	Fuzzy
	Min. convergence time [s]	19.2	35.5	42.6	Fuzzy
	Max. convergence time [s]	29.5	157.2	51.7	Fuzzy
	Mean residual error	3e-3	3e-3	2e-3	PIDm
	Mean power consumed [W·s]	11.8	47.6	22.8	Fuzzy
	Min. power consumed [W·s]	9.3	29.1	15.9	Fuzzy
	Max. power consumed [W·s]	16.2	69.1	27.8	Fuzzy

As can be seen from the table, the Fuzzy controller far outperforms the classic PID controller except from the residual error. The use of the integral error has a number of drawbacks in this system but makes the residual error of the controller smaller compared to the Fuzzy. As can be deduced from the parameters of the membership functions (see Figure 6); the fuzzy controller stops completely when |Z error signal| < 0.01 and |Z gyro signal| < 2.8, resulting in any value less than 0.01 being an immutable error value over time. However, the improvements offered by the Fuzzy controller in terms of convergence time (from 17% to 88% less time) and in terms of energy consumed (from 45% to 86% less energy) are obvious. Besides the convergence and power features, the major difference between the two controllers is the superior ability of the Fuzzy controller to handle variations in boundary conditions achieving reasonably uniform behaviour compared to the classic PID.

DOI: 10.13009/EUCASS2019-386

The same statements can be made in favour of the Fuzzy controller when compared to the modified PID. The latter achieves better performance in terms of residual error. However, the differences are not as great:

- Improvements in convergence time range from 30% less time.
- The best modified PID maneuver consumes 2% less energy than the worst Fuzzy maneuver. However, considering the average of all the maneuvers the Fuzzy consumes 50% of what the modified PID consumes.

In addition, it is important to highlight the improvement achieved when comparing the classic PID with the modified one. In average terms, the modified PID surpasses the classic PID on every account. Excluding the calibration maneuver in which the classic PID is better, the modified PID has managed to adapt correctly to changes in command amplitude, different directions of rotation and the different initial conditions of the maneuvers.

5. Conclusions

In this work the design and implementation of three attitude controllers for a laboratory nanosatellite have been presented. One of them applies the classical concepts of the PID control theory, another slightly modifies the PID strategy and the last one implements an algorithm control based on Fuzzy logic. After briefly presenting the system, a series of maneuvers have been evaluated to analyse the performance of the different controllers in terms of convergence time, accuracy, consumption and robustness.

The first conclusions drawn in relation to the Fuzzy controller are the following:

- Variability in operating conditions slightly affects the response profile of the controller. The overall performance is reasonably uniform, resulting in a robust controller.
- A great improvement of the fuzzy controller is manifested in terms of convergence time. By achieving stability in less time, the energy consumed by the controller is also lower.
- The fact of not using any mechanism which accounts for the integral function makes the Fuzzy controller behave worse in terms of accuracy. The residual error of the Fuzzy controller is always less than 0.01 but any stable situation below that error generates a constant residual error over time.

The conclusions related to the PID controllers used in this system can be summarized in the following points:

- The intrinsic variability of the system due to the non-uniformity of the friction torque and the magnetic field penalizes the performance of a PID controller due to its unique calibration characteristics.
- The modification of the PID strategy in the construction of the integral function worsens the general performance of the controller for the calibration maneuver. However it solves the problem of variations in the response when operating conditions are not exactly the same as in the calibration maneuver.
- Classic PID controller performs generally well for the calibration maneuver.
- The use of the integral function improves the accuracy of the PID controllers by reducing residual error efficiently compared to the Fuzzy controller.

As future work, the ESAT attitude control can be improved following several lines:

- Improvements related to the PID controller:

Knowing the variability of the behaviour of the PID controller depending on the direction of rotation it is possible to solve the problem by generating two completely different sets depending on the direction of rotation in which it is commanded. This solution would improve the response in terms of convergence time and energy consumed, at the cost of spending more time in the calibration of the controller.

Keeping in mind the problems related to the non-uniformity of the magnetic field, it is also possible to explore the possibility of adjusting the PID gains according to the initial position of the system. In this way we would have multipliers that would change their values depending on the magnetic field value in the vicinity of the magnetorquers.

In addition to the criterion of cancelling the integral function, it is possible to study the possibility of introducing other criteria that improve the performance of the PID: a deadband around the commanded state, an angular speed limit above which to brake the rotation, a system of torque graduation according to the battery state of charge, etc.

- Improvements related to the Fuzzy controller:

The same improvements that have been mentioned related to the PID controller could be applied to the Fuzzy controller. In the case of this controller the way to introduce the variability with the direction of rotation is to make the functions of the controller not symmetrical (see Figure 6) so that it responds differently to positive or negative errors.

DOI: 10.13009/EUCASS2019-386

To deal with the non-uniformity of the magnetic field it is possible to introduce a new variable in the fuzzy controller: the measurement of the magnetic field. With this we can fuzzify a new variable and take it into account within our rules to calculate the necessary action. The same concept of introducing new fuzzy variables in the controller can be applied to the control of any other relevant variable such as the battery remaining state of charge.

- New adaptive development:

Taking into account the particularities of the ESAT test environment, it is possible to improve the performance of all controllers by introducing an initial calibration block. Due to the non-controllable variables of this system (progressive wear of the Turntable-Vertical Support joint, differences in system centering leading to differences in the inertia matrix, differences in the position of the magnets, etc.) a self-calibration system seems to be needed. It should, initially, adjusts all the control parameters properly. For this it is necessary to execute a series of maneuvers that include a reasonable sample of the system.

The greatest exponent of this strategy is a learning block which evaluates the performance of the controller "on the loop" by continuously adjusting the control parameters. These systems are known as adaptive controllers.

References

[1] Harland, D. M. and Lorenz, D. R. D. 2005Space Systems Failures, Praxis.

[2] Sidi, M. J., 2000, Spacecraft Dynamics and Control: A practical Engineering Approach. Cambridge University Press.

[3] Gadelha de Souza, L. C. 2006. Design of Satellite Control System Using Optimal Nonlinear Theory. *Mech. Based Des. Struc. and Machines*, 34(4):351–364.

[4] Steyn, W. H., 1994. Comparison of Low-Earth-Orbit Satellite Attitude Controllers Submitted to Controllability Constraints. *J. Guid. Control Dyn*, 17(4): 795-804.

[5] Nagi, F., Ahmed, S., Abidin, A. and Nordin, F., 2010. Fuzzy bang-bang relay controller for satellite attitude control system. *Fuzzy Sets Syst.*, 161:2104-2125.

[6] Guana, P., Liub, X.-J., and Liub, J.-Z., 2005. Adaptive fuzzy sliding mode control for flexible satellite, *Eng Appl Artif. Intel*, 18: 451-459.

[7] Walker, A.R., Putman, P.T. and Cohen, K., 2015. Solely Magnetic Genetic/Fuzzy-Attitude-Control Algorithm for a CubeSat. *J Spacecr. Rockets*, 52(6):1627-1639.

[8] Cheng, C., Shu, S. and Cheng, P., 2009. Attitude control of a satellite using fuzzy controllers. *Expert Syst Appl.*, 36:6613–6620.

[9] Zou, A., Dev Kumar, K. and Hou, Z., 2010. Quaternion-Based Adaptive Output Feedback Attitude Control of Spacecraft Using Chebyshev Neural Networks. *IEE Transactions on Neural Networks*, 21(9):1457-1471.

[10] Fazlyab, A. R., Saberi, F. F. and Kabganian, M., 2016. Adaptive attitude controller for a satellite based on neural network in the presence of unknown external disturbances and actuator faults. *Adv. Space Res.*, 57(1):367-377.

[11] Calvo, D., Avilés, T., Lapuerta, V. and Laverón-Simavilla, A., 2016. Fuzzy Attitude Control for a Nanosatellite in Low Earth Orbit, *Expert Syst Appl*., 58:102-118.

[12] Chulliat, A., S. Macmillan, P. Alken, C. Beggan, M. Nair, B. Hamilton, A. Woods, V. Ridley, S. Maus and A. Thomson, 2015, The US/UK World Magnetic Model for 2015-2020: Technical Report, National Geophysical Data Center, NOAA, 3:47-63.

[13] Diebel, J. 2006. Representing Attitude: Euler Angles, Unit Quaternions, and Rotation Vectors, Matrix, 58(15-16):1-35.

[14] Keat, J. 1977. Analysis of Least-Squares Attitude Determination Routine DOAOP, A:A1-A52. Computer Sciences Corporation Report CSC/TM-77/6034.

[15] Haessig, D.A. and Friedland, B. 1990. On the Modeling and Simulation of Friction. *1990 American Control Conference*, pp. 1256-1261.

[16] Takagi, T. and Sugeno, M. 1985. Fuzzy identification of systems and its applications to modelling and control. *IEEE Transactions on Systems, Man, and Cybernetics*, 15(1):116-132.